doi:10.1093/brain/awab117 BRAIN 2021: 144; 2648–2658 | 2648

BRAIN
ORIGINAL ARTICLE

Somatic *MAP3K3* and *PIK3CA* mutations in sporadic cerebral and spinal cord cavernous malformations

Tao Hong,[1,†] Xiao Xiao,[2,†] Jian Ren,[1,†] Bing Cui,[2] Yuru Zong,[2] Jian Zou,[3] Zqi Kou,[3] Nan Jiang,[1] Guolu Meng,[1] Gao Zeng,[1] Yongzhi Shan,[1] Hao Wu,[1] Zan Chen,[1] Jiantao Liang,[1] Xinru Xiao,[1] Jie Tang,[1] Yukui Wei,[1] Ming Ye,[1] Liyong Sun,[1] Guilin Li,[1] Peng Hu,[1] Rutai Hui,[2] Hongqi Zhang[1] and Yibo Wang[2]

[†]These authors contributed equally to this work.

Cavernous malformations affecting the CNS occur in ~0.16–0.4% of the general population. The majority (85%) of cavernous malformations are in a sporadic form, but the genetic background of sporadic cavernous malformations remains enigmatic. Of the 81 patients, 73 (90.1%) patients were detected carrying somatic missense variants in two genes: *MAP3K3* and *PIK3CA* by whole-exome sequencing. The mutation spectrum correlated with lesion size ($P = 0.001$), anatomical distribution ($P < 0.001$), MRI appearance ($P = 0.004$) and haemorrhage events ($P = 0.006$). *PIK3CA* mutation was a significant predictor of overt haemorrhage events ($P = 0.003$, odds ratio = 11.252, 95% confidence interval = 2.275–55.648). Enrichment of endothelial cell population was associated with a higher fractional abundance of the somatic mutations. Overexpression of the *MAP3K3* mutation perturbed angiogenesis of endothelial cell models and zebrafish embryos . Distinct transcriptional signatures between different genetic subgroups of sporadic cavernous malformations were identified by single cell RNA sequencing and verified by pathological staining. Significant apoptosis in *MAP3K3* mutation carriers and overexpression of *GDF15* and *SERPINA5* in *PIK3CA* mutation carriers contributed to their phenotype. We identified activating *MAP3K3* and *PIK3CA* somatic mutations in the majority (90.1%) of sporadic cavernous malformations and *PIK3CA* mutations could confer a higher risk for overt haemorrhage. Our data provide insights into genomic landscapes, propose a mechanistic explanation and underscore the possibility of a molecular classification for sporadic cavernous malformations.

1 Department of Neurosurgery, Xuanwu Hospital, Capital Medical University, China International Neuroscience Institute, Beijing, China
2 State Key Laboratory of Cardiovascular Disease, Fuwai Hospital, National Center for Cardiovascular Diseases, Chinese Academy of Medical Sciences and Peking Union Medical College, Beijing, China
3 The Institute of Translational Medicine, Zhejiang University, Hangzhou 310058, China

Correspondence to: Yibo Wang, PhD
Fuwai Hospital, Chinese Academy of Medical Sciences and Peking Union Medical College
167 Beilishi Rd, Beijing 100037, China
E-mail: yibowang@hotmail.com

Received December 24, 2020. Revised March 01, 2021. Accepted March 07, 2021. Advance access publication March 17, 2021

Correspondence may also be addressed to: Hongqi Zhang, MD, PhD
Department of Neurosurgery, Xuanwu Hospital
Capital Medical University, 45 Changchun St, Beijing, 100053, China
E-mail: xwzhanghq@163.com

Keywords: MAP3K3; PIK3CA; somatic mutation; cavernous malformations; haemorrhage

Abbreviations: CM = cavernous malformation; ddPCR = droplet digital polymerase chain reaction; WES = whole-exome sequencing

Introduction

Cavernous malformations (CMs) are among the most prevalent vascular malformations affecting the CNS and occur in ~0.16–0.4% of the general population.[1–3] CMs can present incidentally, with seizures or focal neurological deficits most frequently due to haemorrhages.[4] Neurosurgical resection remains the only effective treatment, which is limited by lesion accessibility and is associated with non-negligible rates of morbidity and mortality.[5,6] CMs tend to fall into two categories: familial (inherited) forms and sporadic forms, with the majority (85%) being sporadic.[7,8] The genetic analysis of CMs was mostly based on the inherited form of CMs and was associated with three distinct loci: CCM1 (*KRIT1*), *CCM2* and CCM3 (*PDCD10*).[9–11] Heterozygous loss-of-function of these three mutations was identified in ~90% of familial cases.[5] Previous genetic studies on sporadic CMs mainly focused on the known three CCM genes using PCR amplicons, while the detection rate of pathogenic mutations was low.[12–14] The genetic background of sporadic CMs remains unclear. Recently, pathogenic somatic mutations have been identified in sporadic arteriovenous malformations, capillary malformations, lymphatic malformations and some types of venous malformations.[15–19] We hypothesized that sporadic CMs also arise from somatic mutations in the vasculature of the CNS.

Materials and methods

Study populations

We used whole-exome sequencing (WES) to detect potential pathogenic somatic mutations within the CM lesions and evaluate the possibility of correlating molecular subgroups with clinical characteristics. Patients were eligible for inclusion if they had cerebral or spinal cord CMs with negative family history. The diagnosis of CM was based on the typical appearance of the lesion on MRI and pathological examination of resected samples. Catheter angiography was not used in the evaluation of CMs, unless a differential diagnosis of arteriovenous malformation is being considered. Ninety patients with CMs in the CNS who underwent surgical resection of the lesions at the Beijing Xuanwu Hospital in China between May 2017 and November 2019 were recruited to this study. The study was approved by the ethics committee of Beijing Xuanwu Hospital (no. 2016032) and written informed consent from all patients or their guardians was obtained before surgery.

Clinical characteristics

All medical information was extracted from a computerized online database, which contained demographics, clinical, radiological, and treatment-related information. We defined a haemorrhage event as a symptomatic event with radiographic evidence of overt haemorrhage.[6] The observational period of haemorrhage was defined as the interval between the initial diagnosis and surgical treatment. The MRI appearance of CMs were classified into three types based on the Zabramski classification.[15] Type I was defined as lesions with high signal intensity cores on T_1-weighted imaging and high/low signal intensity on T_2-weighted imaging. Type II was defined as lesions with reticulated, mixed-signal intensity cores on T_1- and T_2-weighted imaging (with surrounding dark rim). Type III was defined as lesions with iso-to-low signal intensity on T_1-weighted imaging and low signal intensity on T_2-weighted imaging. All films were reviewed by independent neuroradiologists. The Karnofsky Performance Scale score was used to provide an objective measure defining neurological functional status of the patients with cerebral or spinal cord CMs. The neurological status of patients with spinal cord CMs were further assessed by the modified McCormick scale.[16]

Genetic analysis and functional studies

We performed WES on fresh-frozen tissue samples of CMs. Sequencing depth was anticipated to be 200–300× for tissue samples. We confirmed the results with droplet digital PCR (ddPCR) analysis to observe mitogen-activated protein kinase kinase kinase 3 (*MAP3K3*) mutation and phosphatidylinositol-4,5-bisphosphate 3-kinase catalytic subunit α (*PIK3CA*) mutations. We also compared variant frequencies of the somatic mutations in endothelial cells and non-endothelial cells of tissue samples using fluorescence-activated cell sorting (FACS) and ddPCR. The functional studies of *PIK3CA* on endothelial cells and animal models have been well performed in previous studies on venous malformations.[17,18] We explored the functions of the *MAP3K3* (p.Ile441Met) mutation in human umbilical vein endothelial cells (HUVECs) and in a zebrafish model.

Single cell transcriptome analysis

Single cell RNA sequencing analyses (10× Genomics) were performed in six samples of sporadic CMs with somatic mutations of *MAP3K3* and/or *PIK3CA* and three control samples. Protein expression was assessed with immunofluorescence staining of tissues.

Statistical analysis

We used Fisher's exact test or Pearson's χ^2 test for categorical variables and Student's -test for continuous variables. Logistic regression analysis was used to assess the impact of multiple variables that predicted an overt haemorrhage event. Cumulative rates of haemorrhage during follow-up were illustrated using the Kaplan-Meier method, and the curves were compared by the log-rank test. All analyses were performed under the guidance of a statistician using SPSS software (version 25, IBM Corp., Armonk, New York, USA). All *P*-values are two-sided, and we defined statistical significance as $P < 0.05$.

Data availability

The authors confirm that the data supporting the findings of this study are available within the article and its Supplementary

material. Derived data supporting the findings of this study are available from the corresponding author on request.

Results

Baseline characteristics of the patients

Ninety consecutive patients were included in the study. WES was performed in 90 fresh-frozen tissue samples of cerebral or spinal cord CMs and two associated cutaneous CMs (Patients 45 and 75). Among these, nine patients were excluded because of carrying germline non-synonymous mutations of *KRIT1* (5/9), *CCM2* (3/9) and *PDCD10* (1/9) by WES. Samples from 81 sporadic patients were eligible for final analysis, including 36 cerebral CMs and 45 spinal cord CMs. Among the 81 patients, 43 (53.1%) were male. The mean age on admission was 37.9 ± 15.7 years (ranging from 3 to 82 years). The clinical characteristics of the patients are summarized in Supplementary Table 1 and Supplementary Fig. 1.

Observation of *MAP3K3* and *PIK3CA* somatic variants in patients

Of the 81 sporadic patients, WES and ddPCR resulted in the identification of somatic missense variants in *MAP3K3* and *PIK3CA* in 73 (90.1%) patients (Fig. 1 and Supplementary Fig. 2). The finding of ddPCR was consistent with the results of WES (= 0.882, $P < 0.001$). Among the 73 patients, 42 (57.5%) were detected as having an *MAP3K3* missense variant (RefSeq accession number NM_002401.3, c.1323C > G, p.Ile441Met) with variant frequencies ranging from 0.4% to 22.7%. The same somatic mutation has been identified in verrucous venous malformations with mutant allele frequencies ranging from 6% to 19% in affected tissue.[19] WES of the associated cutaneous CMs in two patients with spinal cord CMs demonstrated the same *MAP3K3* mutations (p.Ile441Met) as the spinal cord CMs. *PIK3CA* hotspot activating mutations were detected in 45 (61.6%) of the 73 patients, with variant frequencies ranging from 0.4% to 24.4%. *PIK3CA* (NM_006218.2) mutations were found in exon 7: c.1258T > C (p.Cys420Arg), in exon 9: c.1624G > A (p.Glu542Lys), c.1633G > A (p.Glu545Lys); and in exon 20: c.3140A > G (p.His1047Arg). Herein, 14 (19.2%) of the 73 sporadic patients had co-occurred somatic mutations in *MAP3K3* and *PIK3CA*. Genomic coordinates and reference genome of each mutation are described in Supplementary Table 2. For simplicity, we used p.I441M, p.C420R, p.E542K, p.E545K and p.H1047R in this manuscript when referring to these mutations, respectively. Of the samples from the 81 patients with sporadic CMs, we did not find any somatic non-synonymous mutations of the three CCM genes (*KRIT1*, *CCM2* and *PDCD10*).

The somatic mutation genotype was associated with clinical phenotype, especially in haemorrhage

We compared the clinical characteristics of the 73 patients with somatic mutations of *MAP3K3* and/or *PIK3CA* (Tables 1 and 2). Notably, we found that mutational profiles were correlated with risk of haemorrhage events ($P = 0.006$; Table 1 and Fig. 2A). Regarding overt haemorrhage events, a univariate analysis revealed that *PIK3CA* mutations were associated with a statistically significant increase in the likelihood of overt haemorrhage events [$P = 0.002$, odds ratio (OR) = 6.182, 95% confidence interval (CI) = 1.913–19.974; Table 2]. In the multivariate analysis, *PIK3CA* mutations were still a significant predictor of overt haemorrhage events ($P = 0.003$, OR = 11.252, 95% CI = 2.275–55.648; Table 2). Using the log-rank test for haemorrhage-free survival, we noted statistically significantly higher incidence of haemorrhagic events during follow-up in lesions with *PIK3CA* mutations than those with *MAP3K3* mutations ($P = 0.012$; Fig. 2B). The haemorrhagic risk during the follow-up period of the double mutation group was in-between, as expected; however, the *P*-value for the difference between the three genotypes did not achieve statistical significance, though a trend was observed ($P = 0.051$; Fig. 2B).

The mutations spectrum was also correlated with anatomical distribution ($P < 0.001$), size of lesions ($P = 0.001$), and the MRI appearance ($P = 0.004$). The *MAP3K3* mutation was predominantly identified in 80.5% of spinal cord CMs and 31.2% of cerebral CMs. The size of lesions carrying *PIK3CA* mutations was significantly larger ($P = 0.001$; Table 1) than the other two genotypes. The majority (60.0%) of patients with *PIK3CA* mutations had a Zabramski type I appearance of MRIs. While in patients with *MAP3K3* mutations, only 28.6% had a Zabramski type I appearance. In patients with co-occurred mutations, Zabramski type II (53.3%) was the dominant MRI appearance.

The somatic mutations mainly occurred in CD31 + cells

To identify the types of cells that have *MAP3K3* or *PIK3CA* mutations in CMs, we used FACS to sort CD31 + cells (endothelial cell) and CD31– cells from four fresh samples derived from cerebral and spinal cord CMs (Fig. 3A and Supplementary Fig. 3). The ddPCR analysis showed that the CD31 + cells derived from the four samples all had a higher fractional abundance of mutations in *MAP3K3* (I441M) or *PIK3CA* (H1047R), which indicated that the somatic mutations mainly occurred in endothelial cells (Fig. 3A and Supplementary Fig. 4).

MAP3K3 mutation showed an impact on angiogenesis

Cells transfected with *MAP3K3* (I441M), as compared with the control, showed significant activation of phosphorylated ERK5, JNK and p38 (Fig. 3B). However, the extracellular signal-regulated kinase1/2 (ERK1/2) activation was not found. Upregulated *KLF2* and *KLF4* were reported in previous studies,[20] but no significant difference was observed in our results (Supplementary Fig. 5A and C–H). Overexpression of *MAP3K3* (I441M) increased cell proliferation and cell migration ($P < 0.001$) with VEGFA (20 ng/ml) stimulation compared with the control group (Fig. 3C). On cell tube formation, overexpression of the mutation in HUVECs led to disruption and disordering of spontaneous vascular tube formation ($P = 0.001$), with significant reductions of total vascular tube length and total mesh area (Fig. 3D). On cell senescence, overexpression of the *MAP3K3* mutation evidently modified endothelial cell morphology and increased the amount of β-galactosidase (a recognized senescence marker) positive cells (Supplementary Fig. 6 and E). The activating functions of mutations in *PIK3CA* were also performed and overexpression of mutations in *PIK3CA* also promoted cell proliferation, migration, senescence and disrupted tube formation compared with wild-type (Supplementary Figs 5B and 6).

Validation of the impact of *MAP3K3* mutation on angiogenesis in a zebrafish model

To investigate the loss-of-function of Map3k3 in a zebrafish model, morpholino oligonucleotides (MOs) were designed to knockdown wild-type *MAP3K3* in zebrafish embryos. We observed that all of the embryos died within 48 h post-fertilization (hpf) (MO concentration range: 0.05–5 ng), which indicated an indispensable role of Map3k3 in zebrafish embryonic development. Subsequently, to investigate the function of the *MAP3K3* (I441M) mutation, we

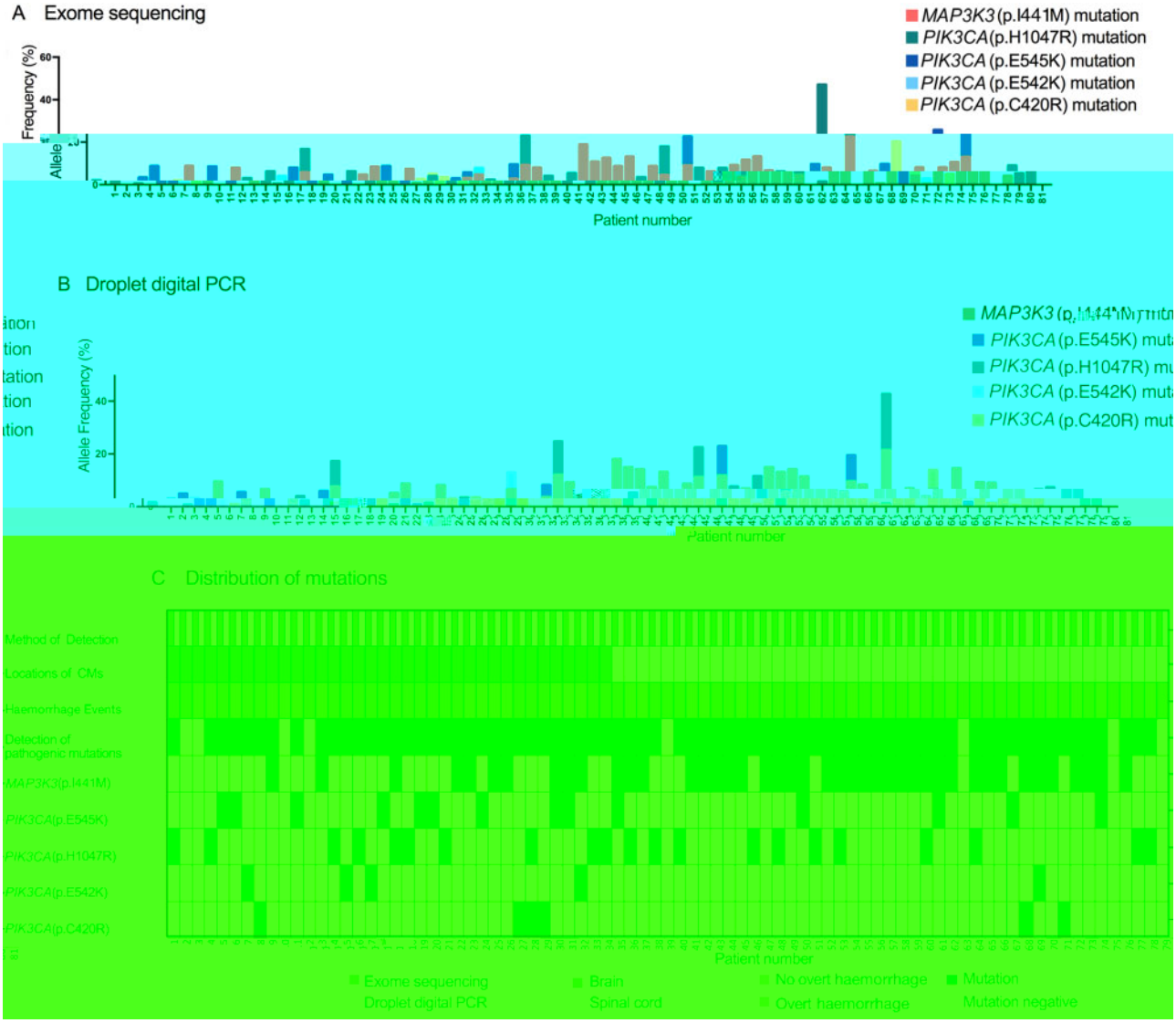

Figure 1 Detection of pathogenic mutations in samples obtained from patients with CMs. (**A**) The detection and allele frequency of the pathogenic mutations on WES. Of the 81 sporadic patients detected, 73 (90.1%) were identified as having pathogenic somatic mutations in *MAP3K3* and/or *PIK3CA*. (**B**) Confirmation and allele frequency of *MAP3K3* and *PIK3CA* mutations by ddPCR. The ddPCR findings were consistent with the WES results (= 0.882, $P < 0.001$). (**C**) Detailed information regarding the tissue samples. The patient number is in order of the CM locations.

injected wild-type and *MAP3K3* (I441M) mRNAs into zebrafish embryos. As expected, in the control group injected with PBS, the upper blood vessels were neatly distributed and the density was uniform. However, in the experimental group injected with wild-type or *MAP3K3* (I441M) mRNAs, part of the upper blood vessels were absent and the blood vessel density was uneven (Fig. 3E). Overexpression of the *MAP3K3* (I441M) mutation caused more severe phenotypes than wild-type mRNA in zebrafish at the same concentration ($P < 0.05$) (Fig. 3F). The observations of endothelial cell models and zebrafish embryos suggested that the *MAP3K3* (I441M) mutation was an activating mutation.

Single cell RNA sequencing revealed distinct transcriptional signatures between *MAP3K3* and *PIK3CA* mutations

In single cell RNA sequencing, 74 326 single cells from nine samples (six CMs samples and three control samples) were profiled and 65 297 cells passed stringent quality control filters for further processing. The six samples of CMs included two CMs with *MAP3K3* mutations (one with cerebral CMs, one with associated cutaneous CMs), three cerebral CMs with *PIK3CA* mutations, and one with cerebral CMs with double mutations. The cutaneous lesion was from Patient 75 with spinal cord CMs at the same spinal metameric segment (Table 3).

The entire population was classified into three cell types, including endothelial cells, mural cells and other cells based on their respective molecular features: *VWF*, *CLDN5*, *CDH5* (endothelial cells) and *PDGFRB*, *ACTA2*, *PDLIM3* (mural cells) (Fig. 4A and B).[21–23] 'Other cells' were identified as mast cells, astrocytes, plasmacytoid dendritic cells (pDCs), B cells, natural killer (NK) cells, dendritic (DC) cells, oligodendrocytes, microglias, macrophages/monocytes, epithelial cells and T cells by interrogating the expression patterns of known marker genes (Fig. 4A and Supplementary Fig. 7).[24–27] Interestingly, all three CM samples with *PIK3CA* mutations had minimal counts of endothelial cells and ratio to the total number of sample cells (Fig. 4C). Most differentially expressed genes (DEGs) in endothelial cells were consistent in different

Table 1 Clinical characteristics and genotype of 73 sporadic CMs patients with somatic mutations

Variable	Overall	Genotype			
		MAP3K3 mutation	*PIK3CA* mutation	Co-occurred mutations	P-value
Patients, (%)	73	28 (38.4)	30 (41.1)	15 (20.5)	
Female, (%)	31 (42.5)	13 (46.4)	14 (46.7)	4 (26.7)	0.366
Mean age at onset ± SD (range), years	36.3 ± 14.4 (8–75)	33.6 ± 14.6 (8–64)	38.1 ± 13.1 (10–58)	37.9 ± 16.8 (9–75)	0.423
Duration of symptoms ± SE, months	22.4 ± 4.4	26.3 ± 8.0	14.7 ± 4.9	30.5 ± 12.1	0.303
Locations of presenting or largest CMs (%)					< 0.001
Supratentorial lobar and cerebellum	18 (24.7)	3 (10.7)	11 (36.7)	4 (26.7)	
Supratentorial deep (basal ganglia/thalamus) and brainstem	14 (19.2)	3 (10.7)	11 (36.7)	0 (0.0)	
Spinal cord	41 (56.2)	22 (78.6)	8 (26.7)	11 (73.3)	
Mean size of CMs ± SD, mm	14.0 ± 8.3	11.1 ± 7.7	17.9 ± 8.7	11.9 ± 5.5	0.001
MRI appearance					0.004
Type I	33 (45.2)	8 (28.6)	18 (60.0)	7 (46.7)	
Type II	27 (37.0)	10 (35.7)	9 (30.0)	8 (53.3)	
Type III	13 (17.8)	10 (35.7)	3 (10.0)	0 (0.0)	
Overt haemorrhage presentation (%)	45 (61.6)	11 (39.3)	24 (80.0)	10 (66.7)	0.006
Mean KPS score ± SD	75.5 ± 16.0	79.6 ± 14.0	74.7 ± 16.3	69.3 ± 17.5	0.076

KPS = Karnofsky Performance Scale.

Table 2 Univariate and multivariate analysis for risk factors of overt haemorrhage in 73 sporadic patients with somatic mutations

Variable	Patients, *n*	Univariate analysis		Multivariate analysis	
		OR (95% CI)	P-value	OR (95% CI)	P-value
Gender	73				
Male	42	Reference		Reference	
Female	31	0.607 (0.234–1.578)	0.306	0.654 (0.211–2.029)	0.462
Age, per each additional year	73	0.991 (0.958–1.024)	0.575	0.987 (0.950–1.026)	0.501
Locations	73		0.271		0.062
Supratentorial and cerebellum	18	Reference		Reference	
Thalamus and brainstem	14	3.667 (0.758–17.728)	0.106	4.634 (0.711–30.220)	0.109
Spinal cord	41	1.563 (0.511–4.774)	0.434	6.073 (1.261–29.245)	0.024
Size, per 0.1 cm increase	73	1.073 (1.001–1.150)	0.048	1.050 (0.968–1.139)	0.238
Genotype	73		0.008		0.008
MAP3K3 mutations	28	Reference		Reference	
PIK3CA mutations	30	6.182 (1.913–19.974)	0.002	11.252 (2.275–55.648)	0.003
Co-occurred mutations	15	3.091 (0.830–11.506)	0.092	4.384 (1.004–19.138)	0.049

comparison groups, which indicated similar general genetic alterations in the sporadic CMs with either *MAP3K3* or *PIK3CA* or both mutations (Fig. 4D). The number of DEGs in different comparisons is shown in Supplementary Fig. 8A. Furthermore, Gene Ontology (GO) analysis of DEGs in three mutation groups versus the control group showed consistency of important pathways such as angiogenesis, blood vessel morphogenesis and blood vessel development (Supplementary Fig. 8B). GO analysis of DEGs between subgroups of *MAP3K3* and *PIK3CA* mutations showed the apoptotic signalling pathway was high ranking (Fig. 4E), which was confirmed by terminal deoxynucleotidyl transferase dUTP nick end labelling (TUNEL) immunostaining of eight samples of sporadic CMs with somatic mutations and three control samples of normal brain tissue. Strong positive staining of apoptosis was observed in endothelial cells of CM samples with *MAP3K3* mutations (= 4), and negative staining was observed in the other two genetic subgroups (three patients with *PIK3CA* mutations, one patient with double mutations) and control samples (= 3), shown in the representative graphs (Fig. 4F). In DEGs between three genetic subgroups and the control group, *GDF15* and *SERPINA5* were notably overexpressed in samples with *PIK3CA* mutations (Fig. 4G), which was consistent with the results following grouping by genotypes (Fig. 4H). These results were also verified by immunofluorescence staining (Fig. 4I).

Discussion

To our knowledge, this is the first study that has demonstrated high prevalence of pathological somatic activating *MAP3K3* and *PIK3CA* mutations in the majority of sporadic CMs in CNS and illustrated the correlations of genotypes with phenotypes. The somatic mutations of *MAP3K3* and *PIK3CA* mainly occurred in endothelial cells. The *MAP3K3* mutations activated the phosphorylated ERK5, JNK and p38 pathway in endothelial cells and caused vascular malformations in zebrafish. Distinct transcriptional signatures between different genetic subgroups were identified. Significant apoptosis in *MAP3K3* mutation carriers and overexpression of *GDF15* and *SERPINA5* in *PIK3CA* mutation carriers contributed to their phenotype.

We did not find any somatic non-synonymous mutations of the three CCM genes (*KRIT1*, *CCM2*, *PDCD10*) in the 81 patients with sporadic CMs. According to previous studies, several somatic mutations in the three CCM genes were found in sporadic CMs,

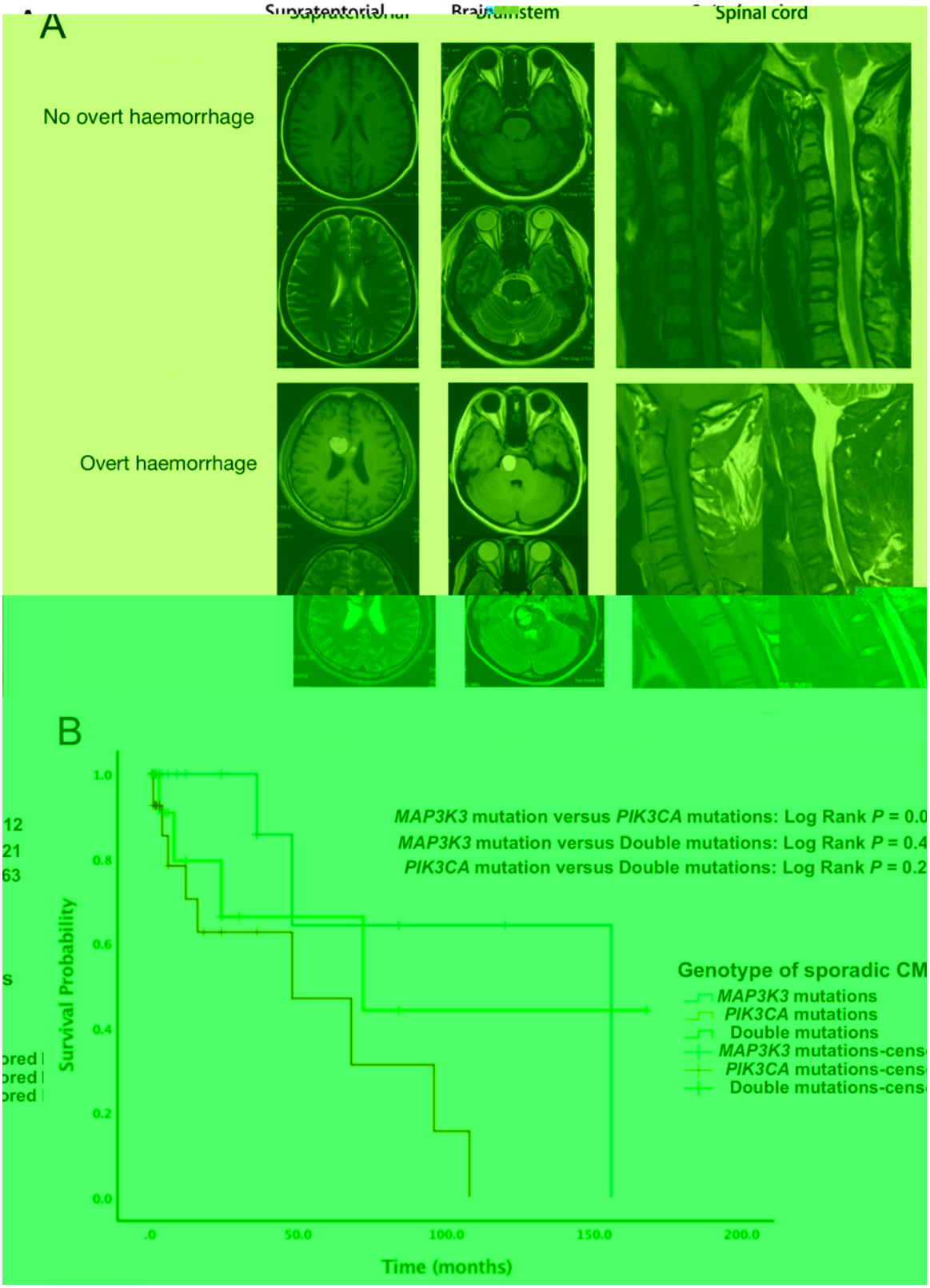

Figure 2 Haemorrhage events of CMs in brain and spinal cord. (**A**) MRI obtained in patients with CMs in lobes, brainstem and spinal cord with/without overt haemorrhage. (**B**) Kaplan-Meier analysis illustrating subsequent haemorrhage risks of sporadic CMs in different genotypes. The log-rank test indicated that haemorrhagic events during the follow-up period were more frequent in patients with *PIK3CA* mutations than with *MAP3K3* mutations ($P = 0.012$) and the haemorrhagic risk during the follow-up period of double mutations was in-between; however, the *P*-value for difference between the three genotypes did not achieve statistical significance, though a trend was observed ($P = 0.051$).

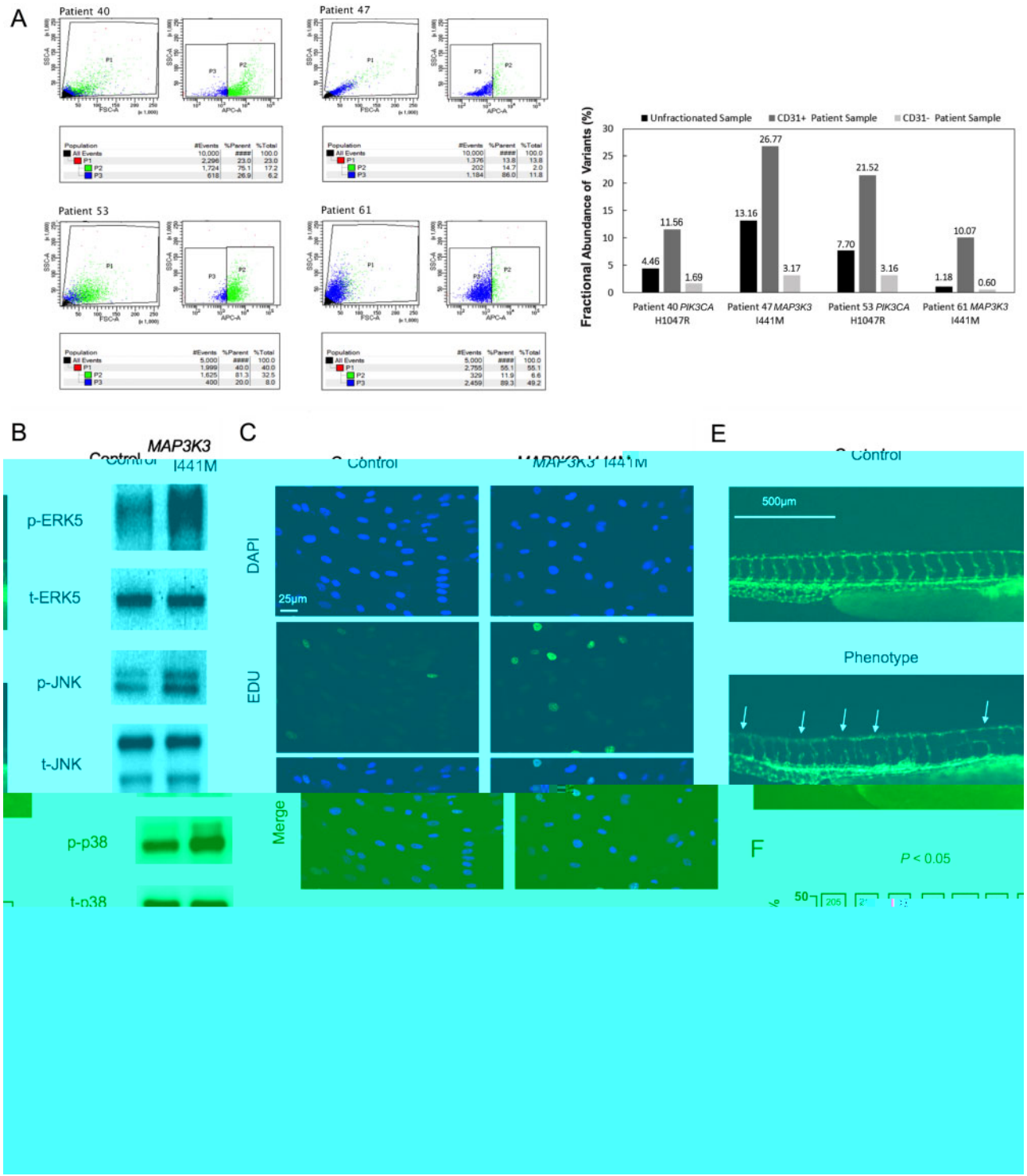

Figure 3 Cell locations of *MAP3K3* and *PIK3CA* mutations and phenotypes of endothelial cells and zebrafish expressing activating Map3k3. (**A**) The FACS plots of flow sorting of four samples of sporadic CMs and the fractional abundance of *MAP3K3* and *PIK3CA* variants in CD31+ and CD31– cells derived from four fresh tissue samples and in the whole tissue sample before sorting. (**B**) Downstream effectors of *MAP3K3*. Plasmids encoding *MAP3K3* (I441M) and wild-type *MAP3K3* (Control) with FLAG-tag were transfected into HUVECs. Significantly increased phosphorylation of extracellular signal regulated kinase 5 (ERK5) was observed with *MAP3K3* (I441M). Increased phosphorylation of p38 and Jun N-terminal kinase (JNK) were also seen with *MAP3K3* (I441M). While no change in phosphorylation of ERK1/2 was observed with the *MAP3K3* (I441M). (**C**) Increased cell proliferation in mutant *MAP3K3* (I441M) compared with wild-type via 5-ethynyl-2'-deoxyuridine (EDU) staining 48 h after transfection and VEGFA (20 ng/ml) treatment for 12 h. Green indicates EDU and blue indicates nucleus [4′,6-diamidino-2-phenylidole dihydrochloride (DAPI)]. (**D**) Visible disruption of endothelial vascular tube formation in cells transfected with mutant *MAP3K3* (I441M) compared with wild-type (Control). (**E**) The vascular deficits of zebrafish injected with wild-type or mutant *MAP3K3* (I441M) mRNA and control (PBS) at 48 h post-fertilization (hpf). The cardiovascular system was marked with EGFP (kdrl). Errors show the locations of absent blood vessels and uneven blood vessel density. (**F**) The quantification of zebrafish with vascular phenotypes (one-way ANOVA test). The number in the box above the column represents the number of patients in each group.

Table 3 Details of donors, tissue region, mutation type, and cell numbers of single cell analysis

Sample	Patient	Donor numbers	Sample type	Somatic mutations	Group	Cell numbers
Sample 1	Patient 28	1	Brainstem CMs	*MAP3K3* I441M	Lesion	7579
Sample 2	Patient 31	1	Brainstem CMs	*PIK3CA* C420R	Lesion	12 414
Sample 3	Patient 32	2	Temporal lobe CMs	*MAP3K3* I441M + *PIK3CA* E545K	Lesion	6743
Sample 4	Patient 32		Control temporal lobe		Control	7568
Sample 5	Patient 35	1	Brainstem CMs	*PIK3CA* H1047R	Lesion	2919
Sample 6	Patient 36	1	Thalamus CMs	*PIK3CA* H1047R	Lesion	6096
Sample 7	Patient 75	2	Associated cutaneous CMs	*MAP3K3* I441M	Lesion	9057
Sample 8	Patient 75		Control skin		Control	4065
Sample 9	Control	1	Control temporal lobe		Control	8856

while the literature quantity was much fewer and the sample size was smaller than those of the familial CMs.[12–14] Regarding the 300× depth of WES in our study, the possibility of finding somatic mutations in these genes in our study was potentially higher than that in some previous studies. We observed the discrepancy of the somatic mutations in the three CCM genes between our study and previous studies on sporadic CMs, which might be due to genetic background from different populations.

Recently, in a cohort of 31 sporadic patients with CMs, five (16.1%) affected individuals were identified carrying heterozygous germline mutations in *RNF213*.[28] However, the majority of sporadic CMs present with single lesions and are non-familial, which indicated an underlying aetiology of somatic rather than germline mutations. Thus, we used WES to detect somatic mutations of low frequency within the CM lesions. Paraffin-fixed samples are prone to singleton changes and other PCR-introduced errors. To avoid bias associated with sample quality and sequencing process, fresh-frozen tissue was obtained during surgical resections and used in WES. Our results identified that 90.1% of sporadic CMs carried pathogenic somatic missense variants in *MAP3K3* and/or *PIK3CA*. We also found cases with concomitant mutations of both *MAP3K3* and *PIK3CA*. Similar co-occurrence of pathogenic mutations in different genes has previously been detected in other types of vascular malformations and cancer.[29,30] In these sporadic CMs with double mutations, the allele frequencies are relatively similar. These results raised an intriguing question regarding whether the mutations occurred in the same cell. Similar abundance is not convincing evidence and the mutations are located far from the 3′ end of the transcripts, rendering them not detectable by the single cell RNA sequencing with short reads. Further studies should be carried out to clarify this.

Previous literature has mostly focused on the genetic background of CCMs in a familial form. The concept of Knudson's two-hit mechanism might play an important role in familial CCM on the basis of the autosomal dominant pattern of inheritance of CCM and the presence of multiple lesions, which have been supported by mouse model of CCM.[13,31–33] Of the 90 consecutive patients included in the present study, WES identified nine patients carrying germline non-synonymous mutations of *KRIT1*/CCM1 (5/9), *MGC4607/CCM2* (3/9) and *PDCD10*/CCM3 (1/9). One patient was detected carrying a germline mutation of *KRIT1* in germline mutant allele and a somatic mutation of *KRIT1* in the wild-type allele of the gene. That is, the CCM tissue showed a somatic mutation in the CCM gene that harbours the germline mutation, the somatic mutation then inactivates the remaining wild-type allele. The finding of this patient with biallelic somatic and germline mutations of *KRIT1* indicated a two-hit mechanism of familial CCM pathogenesis.

Patients with sporadic CMs are heterogeneous, for whom predicting future haemorrhagic and neurological risk remains a challenge.[34] Previous studies have found that prior haemorrhage events and the location of CMs are valuable in predicting haemorrhage.[35,36] We found that in sporadic CMs, the mutation pattern was associated with distinct clinical characteristics. The results were consistent with transcriptomic analysis demonstrating that samples with different genetic mutations had distinct transcriptional signatures. Previous studies have reported that the apoptosis resistance of endothelial cells in pulmonary arterial hypertension promoted vascular obstruction.[37] In our study, transcriptomic analysis as well as immunostaining demostrated that endothelial cells from samples with *PIK3CA* mutations had a low apoptosis rate, indicating that CM lesions with *PIK3CA* mutations might also be susceptible to vascular obstruction. The minimal counts of endothelial cells and apoptosis resistance reflect severe dysfunctions of endothelial cells and impairment of vascular structures in CMs with *PIK3CA* mutations. Moreover, the expression of *SERPINA5* and *GDF15* in pathological level may functionally correlate with the haemorrhagic characteristics of CMs and may represent a biomarker for haemorrhagic risk and predictor of genetypes in CMs. *SERPINA5* (protein C inhibitor, plasminogen activator inhibitor-3) is a secreted, extracellular clade A serpin, which has been related to anticoagulation.[38] The expression of growth differentiation factor 15 (*GDF15*) is increased during endothelial dysfunction, which is in response to a vascular stress and activated by oncogenic *PIK3CA*.[24,19,39] The high prevalence of *MAP3K3* and *PIK3CA* in sporadic CMs and the distinctive clinical characteristics in different genetic subgroups may lead to a new molecular classification of sporadic CMs.

Somatic mutations in the PI3K-AKT-mTOR and RAS-MAPK pathways have been identified in some types of vascular malformations.[19,40–45] Activating mutations of the *MAP3K3* and *PIK3CA* are accompanied by dysregulation of the MAPK-ERK pathway and PIK-AKT-MTOR pathway.[17,18,46,47] Previous studies have shown that MEKK3 was a CCM2 binding partner and CCMs arose from the loss of an adaptor complex (CCM complex) and gain of MEKK3-MEK5-ERK5 signalling in brain endothelial cell.[48] CCM2 is osmosensing scaffold for MEKK3 and modulates the MEKK3-dependent p38 activation.[49] The p38 pathway contributes to the abnormal development of vessels in CMs. Based on the functional studies of the present study, we can infer that MAPK pathway activation plays an important role in both sporadic and familial CMs. These findings may alter the concept of management of these CMs by introducing the possibility of targeted medical therapy in the context of surgical intervention are not always possible.

Taken together, we identified activating *MAP3K3* and *PIK3CA* somatic mutations in the majority (90.1%) of sporadic CMs of the

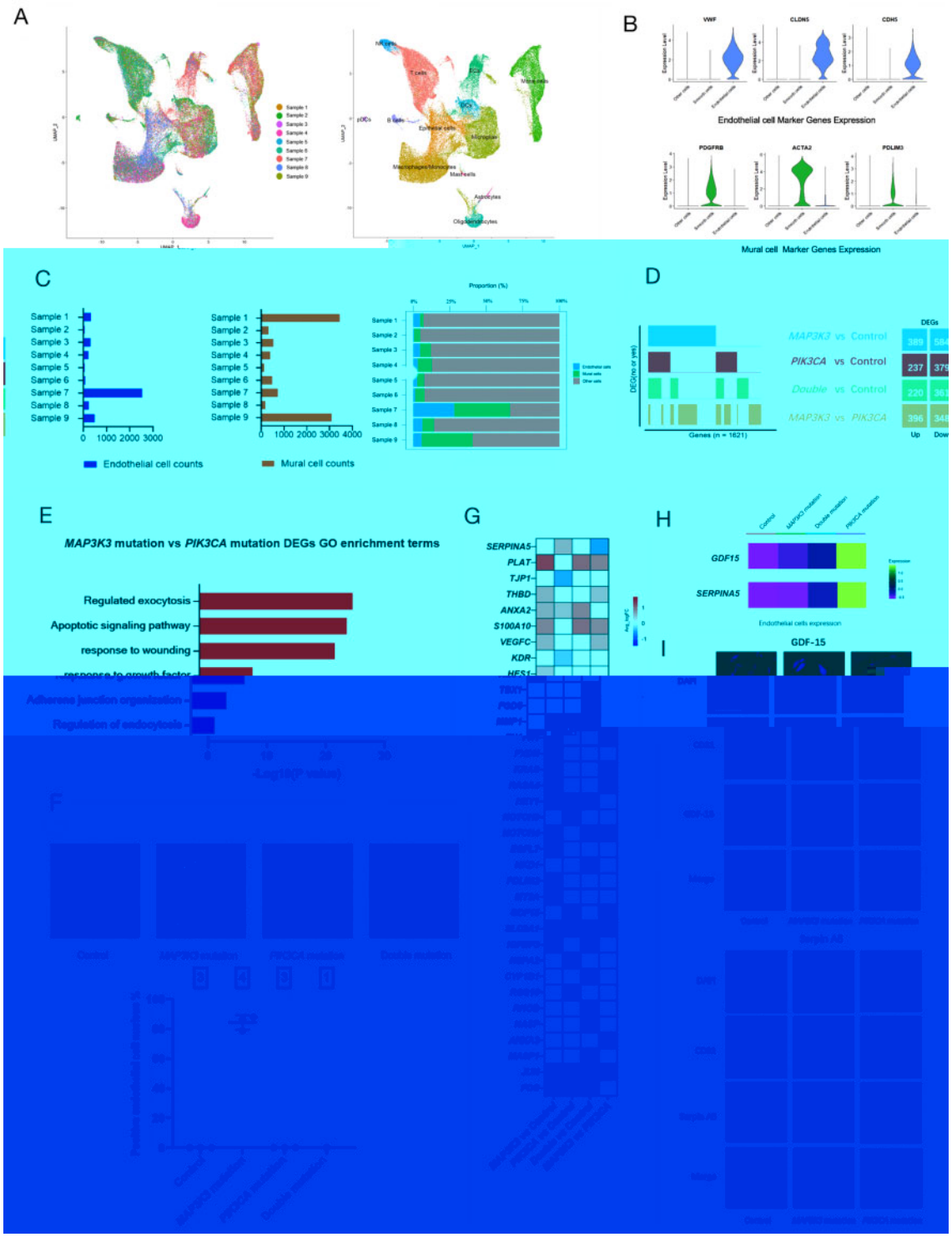

Figure 4 Single cell RNA sequence revealed distinct transcriptional signatures between *MAP3K3* and *PIK3CA* mutations. (**A**) UMAP (uniform manifold approximation and projection) clustering of 65 297 cells isolated from nine samples (six CMs samples and three control samples). Cells were marked by tissue sources (*ef*) or cell types (,). (**B**) Violin plots of endothelial cell and mural cell marker genes expressions identified by differential expression analysis. (**C**) Bar graphs depicting the counts of endothelial cells and mural cells from nine samples. R , : The proportion of endothelial cells, mural cells and other cells. (**D**) Binary plots indicating with bars whether a gene (c) is a differentially expressed gene (DEG) in a given comparison group ( ) or not (= 1621 DEGs). R , : DEG counts for each comparison group. (**E**) Selected top categories from GO enrichment analysis of DEGs to compare the differences of biological functions between *MAP3K3* and *PIK3CA* mutation groups. (**F**) TUNEL immunostaining of CM tissues with *MAP3K3* mutations (Patient 43), *PIK3CA* mutations (Patient 11), double mutations of *MAP3K3* and *PIK3CA* (Patient 66), and one control tissue of temporal lobe. Overlay of DAPI (blue), CD31 (red) and apoptotic nucleus (green) are shown. The quantification of apoptotic endothelial cells from *MAP3K3* mutation groups were much higher than other groups ($P < 0.001$). The number in the box above the column represents the number of patients in each group. *MAP3K3* mutation groups included Patients 13, 43, 45 and 57. *PIK3CA* mutation groups included Patients 11, 22 and 40. The double mutation group included Patient 66. (**G**) Heat maps of the expression of related DEGs from different subgroups compared with the control group. (**H**) Heat maps of *GDF15* and *SERPINA5* expressions in three genetic subgroups and the control group. (**I**) Immunostaining of CM tissues with *MAP3K3* (Patient 5), *PIK3CA* (Patient 45) mutations and control tissue for GDF-15 and Serpin A5. *MAP3K3* mutation groups included Patients 43, 46 and 68. *PIK3CA* mutation groups included Patients 5, 11 and 52. Consistent with the results of single cell RNA sequencing, both were positive in patients of *PIK3CA* mutation and negative in other samples. Single-channel images of DAPI (blue), CD31 (red), GDF-15 (green) or Serpin A5 (green) and overlay of them are all shown.

CNS. The mutations spectrum may correlate with the phenotype of sporadic CMs and *PIK3CA* mutations may confer a higher risk for overt haemorrhage. The functional studies and single cell transcriptomic analysis provide a blueprint for interrogating the cellular and molecular basis of sporadic CMs.

Acknowledgements

We thank all the patients and their families for participating in our study, and for offering all information, data, and updates on the disease in these patients.

Funding

This work was supported by National Key R&D Program of China (2017YFC0909400), National Natural Science Foundation of China with grants (81770424, 81970430, 81971104, 81971113 and 81671202), Chinese Academy of Medical Sciences with Innovation Fund for Medical Sciences Health and Longevity Pilot Project (CIFMS2017-I2M-1-008 and 2019-RC-HL-002), Beijing Municipal Science and Technology Commission (Z201100005520024), Beijing Municipal Administration of Hospitals (DFL2018080 and QML20190802) and Beijing Municipal Education Commission (CIT&TCD201904095).

Competing interests

The authors report no competing interests.

Supplementary material

Supplementary material is available at *Brain* online.

References

1. Vernooij MW, Ikram MA, Tanghe HL, et al. Incidental findings on brain MRI in the general population. *N Engl J Med*. 2007; 357(18):1821–1828.
2. Otten P, Pizzolato GP, Rilliet B, Berney J. 131 cases of cavernous angioma (cavernomas) of the CNS, discovered by retrospective analysis of 24,535 autopsies. *Neurochirurgie*. 1989;35(2):82–131.
3. Morris Z, Whiteley WN, Longstreth WT Jr, et al. Incidental findings on brain magnetic resonance imaging: Systematic review and meta-analysis. *BMJ*. 2009;339(1):b3016.
4. Batra S, Lin D, Recinos PF, Zhang J, Rigamonti D. Cavernous malformations: Natural history, diagnosis and treatment. *Nat Rev Neurol*. 2009;5(12):659–670.
5. Chohan MO, Marchio S, Morrison LA, et al. Emerging pharmacologic targets in cerebral cavernous malformation and potential strategies to alter the natural history of a difficult disease: A review. *JAMA Neurol*. 2019;76(4):492–500.
6. Akers A, Al-Shahi Salman R, Awad IA, et al. Synopsis of guidelines for the clinical management of cerebral cavernous malformations: Consensus recommendations based on systematic literature review by the angioma alliance scientific advisory board clinical experts panel. *Neurosurgery*. 2017;80(5):665–680.
7. Zafar A, Quadri SA, Farooqui M, et al. Familial cerebral cavernous malformations. *Stroke*. 2019;50(5):1294–1301.
8. Flemming KD, Graff-Radford J, Aakre J, et al. Population-based prevalence of cerebral cavernous malformations in older adults: Mayo clinic study of aging. *JAMA Neurol*. 2017;74(7):801–805.
9. Laberge-Le Couteulx S, Jung HH, Labauge P, et al. Truncating mutations in CCM1, encoding KRIT1, cause hereditary cavernous angiomas. *Nat Genet*. 1999;23(2):189–193.
10. Liquori CL, Berg MJ, Siegel AM, et al. Mutations in a gene encoding a novel protein containing a phosphotyrosine-binding domain cause type 2 cerebral cavernous malformations. *Am J Hum Genet*. 2003;73(6):1459–1464.
11. Bergametti F, Denier C, Labauge P, et al.; Société Française de Neurochirurgie. Mutations within the programmed cell death 10 gene cause cerebral cavernous malformations. *Am J Hum Genet*. 2005;76(1):42–51.
12. Gault J, Awad IA, Recksiek P, et al. Cerebral cavernous malformations: Somatic mutations in vascular endothelial cells. *Neurosurgery*. 2009;65(1):138–145.
13. Akers AL, Johnson E, Steinberg GK, Zabramski JM, Marchuk DA. Biallelic somatic and germline mutations in cerebral cavernous malformations (CCMs): Evidence for a two-hit mechanism of CCM pathogenesis. *Hum Mol Genet*. 2009;18(5):919–930.
14. McDonald DA, Shi C, Shenkar R, et al. Lesions from patients with sporadic cerebral cavernous malformations harbor somatic mutations in the CCM genes: evidence for a common biochemical pathway for CCM pathogenesis. *Hum Mol Genet*. 2014; 23(16):4357–4370.
15. Zabramski JM, Wascher TM, Spetzler RF, et al. The natural history of familial cavernous malformations: Results of an ongoing study. *J Neurosurg*. 1994;80(3):422–432.
16. Aghakhani N, David P, Parker F, Lacroix C, Benoudiba F, Tadie M. Intramedullary spinal ependymomas: Analysis of a consecutive series of 82 adult cases with particular attention to patients with no preoperative neurological deficit. *Neurosurgery*. 2008; 62(6):1279–1285.
17. Castel P, Carmona FJ, Grego-Bessa J, et al. Somatic PIK3CA mutations as a driver of sporadic venous malformations. *Sci Transl Med*. 2016;8(332):332ra42.
18. Castillo SD, Tzouanacou E, Zaw-Thin M, et al. Somatic activating mutations in Pik3ca cause sporadic venous malformations in mice and humans. *Sci Transl Med*. 2016;8(332):332ra43.
19. Couto JA, Vivero MP, Kozakewich HP, et al. A somatic MAP3K3 mutation is associated with verrucous venous malformation. *Am J Hum Genet*. 2015;96(3):480–486.
20. Otten C, Knox J, Boulday G, et al. Systematic pharmacological screens uncover novel pathways involved in cerebral cavernous malformations. *EMBO Mol Med*. 2018;10(10):e9155.
21. Kalna V, Yang Y, Peghaire CR, et al. The transcription factor ERG regulates super-enhancers associated with an endothelial-specific gene expression program. *Circ Res*. 2019;124(9): 1337–1349.
22. Smyth LCD, Rustenhoven J, Scotter EL, et al. Markers for human brain pericytes and smooth muscle cells. *J Chem Neuroanat*. 2018;92:48–60.
23. Uhlen M, Fagerberg L, Hallstrom BM, et al. Proteomics. Tissue-based map of the human proteome. *Science*. 2015;347(6220):1260419.
24. Kim JS, Lee C, Bonifant CL, Ressom H, Waldman T. Activation of p53-dependent growth suppression in human cells by mutations in PTEN or PIK3CA. *Mol Cell Biol*. 2007;27(2):662–677.
25. Lake BB, Chen S, Sos BC, et al. Integrative single-cell analysis of transcriptional and epigenetic states in the human adult brain. *Nat Biotechnol*. 2018;36(1):70–80.
26. Mathys H, Davila-Velderrain J, Peng Z, et al. Single-cell transcriptomic analysis of Alzheimer's disease. *Nature*. 2019; 570(7761):332–337.
27. Zhang X, Lan Y, Xu J, et al. CellMarker: A manually curated resource of cell markers in human and mouse. *Nucleic Acids Res*. 2019;47(D1):D721–D728.
28. Lin J, Liang J, Wen J, et al. Mutations of RNF213 are responsible for sporadic cerebral cavernous malformation and lead to a mulberry-like cluster in zebrafish. *J Cereb Blood Flow Metab*. 2020; 41(6):1251–1263.

29. Janku F, Lee JJ, Tsimberidou AM, et al. PIK3CA mutations frequently coexist with RAS and BRAF mutations in patients with advanced cancers. *PL S O e*. 2011;6(7):e22769.
30. Ten Broek RW, Eijkelenboom A, van der Vleuten CJM, et al. Comprehensive molecular and clinicopathological analysis of vascular malformations: A study of 319 cases. *Ge e C e Ca ce*. 2019;58(8):541–550.
31. Pagenstecher A, Stahl S, Sure U, Felbor U. A two-hit mechanism causes cerebral cavernous malformations: Complete inactivation of CCM1, CCM2 or CCM3 in affected endothelial cells. *H M Ge e*. 2009;18(5):911–918.
32. McDonald DA, Shenkar R, Shi C, et al. A novel mouse model of cerebral cavernous malformations based on the two-hit mutation hypothesis recapitulates the human disease. *H M Ge e*. 2011;20(2):211–222.
33. Spiegler S, Rath M, Much CD, Sendtner BS, Felbor U. Precise CCM1 gene correction and inactivation in patient-derived endothelial cells: Modeling Knudson's two-hit hypothesis in vitro. *M Ge e Ge c Med*. 2019;7(7):e00755.
34. Goyal A, Rinaldo L, Alkhataybeh R, et al. Clinical presentation, natural history and outcomes of intramedullary spinal cord cavernous malformations. *J Ne Ne P a*. 2019; 90(6):695–703.
35. Horne MA, Flemming KD, Su IC, et al.; Cerebral Cavernous Malformations Individual Patient Data Meta-analysis Collaborators. Clinical course of untreated cerebral cavernous malformations: A meta-analysis of individual patient data. *La ce Ne*. 2016;15(2):166–173.
36. Al-Shahi Salman R, Hall JM, Horne MA, et al. Untreated clinical course of cerebral cavernous malformations: A prospective, population-based cohort study. *La ce Ne*. 2012;11(3):217–224.
37. Thenappan T, Ormiston ML, Ryan JJ, Archer SL. Pulmonary arterial hypertension: Pathogenesis and clinical management. *BMJ*. 2018;360:j5492.
38. Elisen MG, von D. B P, Bouma BN, Meijers JC. Prote-1.v.406 TD27(l)17.2(a)0(t)1,Ryan 71.82(ke)(7(a)]TJT[ahibiuntrathogenesis)-570.1(and)- -1ata.Thaata.[(.)-